JVI Journals.ASM.org

Nanobody Binding to a Conserved Epitope Promotes Norovirus Particle Disassembly

Anna D. Koromyslova, Grant S. Hansman

Schaller Research Group at the University of Heidelberg and the DKFZ, Germany, Heidelberg, Germany, and Department of Infectious Diseases, Virology, University of Heidelberg, Germany, Heidelberg, Germany

ABSTRACT

Human noroviruses are icosahedral single-stranded RNA viruses. The capsid protein is divided into shell (S) and protruding (P) domains, which are connected by a flexible hinge region. There are numerous genetically and antigenically distinct noroviruses, and the dominant strains evolve every other year. Vaccine and antiviral development is hampered by the difficulties in growing human norovirus in cell culture and the continually evolving strains. Here, we show the X-ray crystal structures of human norovirus P domains in complex with two different nanobodies. One nanobody, Nano-85, was broadly reactive, while the other, Nano-25, was strain specific. We showed that both nanobodies bound to the lower region on the P domain and had nanomolar affinities. The Nano-85 binding site mainly comprised highly conserved amino acids among the genetically distinct genogroup II noroviruses. Several of the conserved residues also were recognized by a broadly reactive monoclonal antibody, which suggested this region contained a dominant epitope. Superposition of the P domain nanobody complex structures into a cryoelectron microscopy particle structure revealed that both nanobodies bound at occluded sites on the particles. The flexible hinge region, which contained ~10 to 12 amino acids, likely permitted a certain degree of P domain movement on the particles in order to accommodate the nanobodies. Interestingly, the Nano-85 binding interaction with intact particles caused the particles to disassemble *in vitro*. Altogether, these results suggested that the highly conserved Nano-85 binding epitope contained a trigger mechanism for particle disassembly. Principally, this epitope represents a potential site of norovirus vulnerability.

IMPORTANCE

We characterized two different nanobodies (Nano-85 and Nano-25) that bind to human noroviruses. Both nanobodies bound with high affinities to the lower region of the P domain, which was occluded on intact particles. Nano-25 was specific for GII.10, whereas Nano-85 bound several different GII genotypes, including GII.4, GII.10, and GII.12. We showed that Nano-85 was able to detect norovirus virions in clinical stool specimens using a sandwich enzyme-linked immunosorbent assay. Importantly, we found that Nano-85 binding to intact particles caused the particles to disassemble. We believe that with further testing, Nano-85 not only will work as a diagnostic reagent in norovirus detection systems but also could function as a broadly reactive GII norovirus antiviral.

Human noroviruses are the most important cause of outbreaks of gastroenteritis. The norovirus genome has three open reading frames (ORF1 to ORF3), where ORF1 encodes the nonstructural proteins, ORF2 encodes the capsid protein (VP1), and ORF3 encodes a small structural protein. The expression of the capsid protein in insect cells leads to the self-assembly of virus-like particles (VLPs) that are morphologically and antigenically similar to the native virions (1). Based on the capsid gene sequences, at least seven genogroups (GI to GVII) have been assigned (2, 3). The genogroups can be further subdivided into numerous genotypes, and an association between genetic clusters and antigenicity is evident (1). However, a single genetic cluster (genogroup GII, genotype 4; GII.4) has dominated over the past decade (4). GII.4 members evolve ~5% every year and are believed to have a mechanism that allows the virus to evade the immune system or alter receptor binding profiles (5–7). Recently, a human norovirus cell culture was developed (8); however, vaccine and antiviral development still is hampered by the large antigenic diversity and the constantly changing strains (1).

The X-ray crystal structure of the GI.1 norovirus VLPs showed that VP1 is divided into two domains, shell (S) and protruding (P) domains (9). The S domain forms a scaffold surrounding the RNA, whereas the P domains extend off the S domain and likely contain the main determinants for strain diversity. There are two other high-resolution cryo-electron microscopy (cryo-EM) structures of norovirus particles, GV.1 murine norovirus and GII.10 human norovirus (10, 11). One major structural distinction among these particles is the position of the P domain on the S domain. In the case of GI.1, the P domain is resting on the S domain, whereas in GV.1 and GII.10, the P domains are raised off the S domain by ~15 Å. In most noroviruses, the S and P domains are connected by a flexible hinge region, ~10 to 12 amino acids long, which likely permits a certain amount of P domain movement on the S domain (12).

Little is known about antibody binding and cross-reactivities

Received 31 October 2014 **Accepted** 12 December 2014

Accepted manuscript posted online 17 December 2014

Citation Koromyslova AD, Hansman GS. 2015. Nanobody binding to a conserved epitope promotes norovirus particle disassembly. J Virol 89:2718–2730. doi:10.1128/JVI.03176-14.

Editor: S. López

Address correspondence to Grant S. Hansman, g.hansman@dkfz.de.

Supplemental material for this article may be found at http://dx.doi.org/10.1128/JVI.03176-14.

doi:10.1128/JVI.03176-14

```
                                  CDR-1                                CDR-2
Nano-25     DVQLVESGGGLVQPGGSLRLSCAASESILSFNHMAWYRQGPGEQRELVAVITREGSTDYA   60
Nano-85     DVQLVESGGGLVQPGGSLRLSCAASGSIFSIYAMGWYRQAPGKQRELVASISSGGGTNYA   60
            ************************** ** *   * **** ** ***** *   *  * **

                                                CDR-3
Nano-25     DSVKGRFTISRDNAKNMVYLLMSNLRPEDTAVYYCNRG-------ISNPWGQGTQVTVSS   113
Nano-85     DSVKGRFTISGDNAKNTVYLQMNSLKPEDTAVYYCKREDYSAYAPPSGSRGRGTQVTVSS   120
            ********** ***** *** *  * ********* *         *   * ********
```

FIG 1 Amino acid alignment of Nano-25 and Nano-85. The nanobody amino acid sequences were aligned using Clustal X. The CDRs (blue bars) were highly variable between Nano-25 and Nano-85. An insertion was found in the Nano-85 CDR-3. The nanobody amino acids involved in P domain binding were colored accordingly: GII.10 Nano-25, green; GII.10 Nano-85, orange. The asterisks represent conserved amino acids.

against norovirus particles at the structural level. We recently solved the first X-ray crystal structure of a norovirus P domain Fab complex (11). Superposition of the P domain Fab complex on the cryo-EM VLP structure showed the Fab bound to an occluded site on the particle, i.e., hindered by neighboring P domains. Interestingly, this broadly reactive monoclonal antibody recognizes a partially conserved region on the P domain and is used in a commercial diagnostic enzyme-linked immunosorbent assay (ELISA) detection kit. Moreover, several other broadly reactive diagnostic monoclonal antibodies are thought to bind this occluded region on particles (13, 14). This suggested the occluded region was accessible on intact particles. In this study, we analyzed the binding characteristics of two norovirus-specific nanobodies, termed Nano-85 and Nano-25. Nanobodies are single-domain antibodies of ~14 kDa which can bind with high affinities to a specific antigen. We showed that both nanobodies bound to the lower regions on the P domain using X-ray crystallography. The nanobody binding regions were occluded on intact particles. Interestingly, Nano-85 binding to intact particles caused the particles to disassemble, which suggested the binding epitope contained a disassembly trigger.

MATERIALS AND METHODS

VLP production and EM. The capsid gene of norovirus GII.10 Vietnam026 (AF504671), GII.12 Hiro (AB044366), GI.1 Norwalk virus (AY502016), and GII.4 NSW-2012 (JX459908) was cloned into a baculovirus expression system as previously described (15, 16). VLPs were harvested at 5 days postinfection. The supernatant was pelletized and applied to a 15 to 45% sucrose-phosphate-buffered saline (PBS) ultracentrifugation gradient (Beckmann SW40-Ti rotor) for 2 h at 4°C. Fractions were confirmed using electron microscopy (EM), and homogenous particles were pooled and concentrated to 2 to 10 mg/ml in PBS (pH 7.4). The VLP samples were applied to EM grids, washed once in distilled water, and then

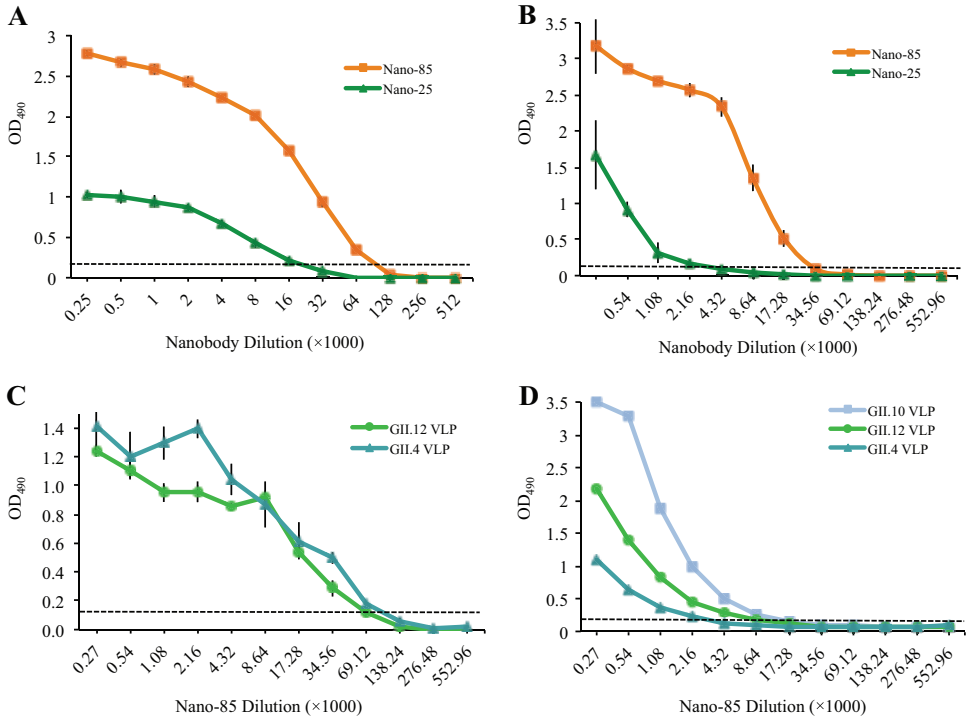

FIG 2 Nanobody binding interactions against norovirus VLPs and P domains were measured using ELISA. All experiments were performed in triplicate (error bars shown), and the cutoff was at an OD_{490} of >0.15 (dashed line). (A) GII.10 VLPs were coated on the plate and detected with serially diluted Nano-85 and Nano-25 using a direct ELISA. Nano-85 and Nano-25 detected GII.10 VLPs at dilutions of 64,000 and 16,000, respectively. (B) GII.10 P domains were coated on the plate and detected with serially diluted Nano-85 and Nano-25 using a direct ELISA. Nano-85 and Nano-25 detected GII.10 P domains at dilutions of 17,280 and 2,160, respectively. (C) GII.4 and GII.12 VLPs were coated on the plate and detected with serially diluted Nano-85 using a direct ELISA. Nano-85 detected GII.4 and GII.12 VLPs at dilutions of 69,120 and 34,560, respectively. (D) For the sandwich ELISA, we used a mixture of monoclonal antibodies as capture and serially diluted Nano-85 as detector. Nano-85 detected GII.10, GII.12, and GII.4 VLPs at dilutions of 17,280, 8,640, and 2,160, respectively.

A

Specimen No.	2	4	5	8	9	12	13	14	15	16
ELISA OD_{490}	0	0.02	0.01	0.62	0	0.15	0.78	0	0.01	0
Specimen No.	17	18	19	21	22	23	24	28	30	31
ELISA OD_{490}	0.18	0.02	0.19	0.06	0.03	0.03	0.02	0.02	0.01	0
Specimen No.	34	35	40	42	43	47	48	49	54	55
ELISA OD_{490}	0	0.04	0	0.5	0.09	0.13	0.38	0.03	0.01	0.43

B

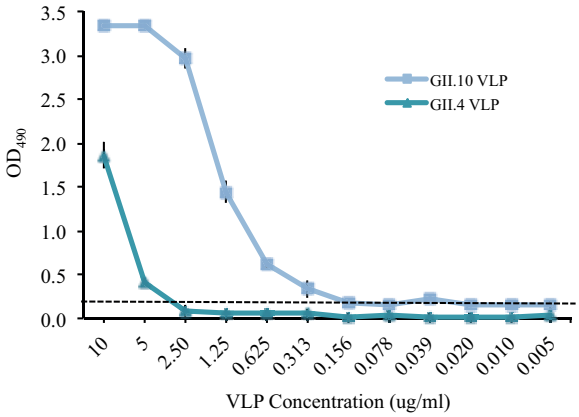

FIG 3 Sandwich ELISA was used to detect norovirus in clinical stool specimens and determine the detection limit. All experiments were performed in duplicate, and the positive reaction/cutoff was at an OD_{490} of >0.2. (A) The sandwich ELISA used a GII.4-specific monoclonal antibody as capture and Nano-85 as detector. Thirty specimens were screened, and 12 were GII.4 norovirus positive using RT-PCR (green). The ELISA-positive specimens (blue) showed the average OD_{490} value. The ELISA detected 4 of 12 RT-PCR-positive specimens and one RT-PCR-negative specimen. (B) The detection limit of a sandwich ELISA was performed with serially diluted GII.4 and GII.10 VLPs, each spiked separately in a 10% stool suspension. A mixture of monoclonal antibodies was used as capture and Nano-85 as detector. The ELISA detected 5 μg/ml and 0.3 μg/ml of GII.4 and GII.10 VLPs, respectively.

stained with 4% uranyl acetate. The samples were examined using EM (Zeiss EM 910).

P domain production. The P domain of GII.10 (Vietnam026), GII.12 (Hiro), GII.4 (Saga-2006), and GII.4 (NSW-2012) was produced as previously described (17). Briefly, the P domain was cloned into a modified expression vector (pMal-c2X; New England BioLabs) and transformed into *Escherichia coli* BL21 cells. Transformed cells were grown at 37°C in LB medium for 2 h. Expression was induced with isopropyl-β-D-thiogalactopyranoside (IPTG) (0.75 mM) at an optical density at 600 nm (OD_{600}) of 0.6 for 18 h at 22°C. Cells were harvested by centrifugation and disrupted by sonication on ice. A His-tagged fusion-P domain protein was eluted from a Ni-nitrilotriacetic acid (NTA) column after a series of washing steps. The fusion protein was digested with HRV-3C protease (Novagen) overnight at 4°C, and then the P domain was separated on the Ni-NTA column and dialyzed in gel filtration buffer (GFB; 0.35 M NaCl and 25 mM Tris-HCl [pH 7.4]) overnight at 4°C. The P domain was further purified by size exclusion chromatography with a Superdex-200 column and stored in GFB at 4°C.

Nanobody production. A single alpaca was injected subcutaneously on days 0, 7, 14, 21, 28, and 35 with ~115 μg GII.10 VLP protein per injection (VIB Nanobody Service Facility, Vrije University, Brussels, Belgium). The alpaca immunization was performed by the VIB Nanobody Service Facility with the approval of the Ethical Commission of Vrije Universiteit, Brussels, Belgium. A VHH library was constructed and screened for the presence of antigen-specific nanobodies. A VHH library of about 10^8 independent transformants was obtained. Three consecutive rounds of panning were performed on a solid-phase coating with GII.10 VLPs (20 μg/well). In total, 143 individual colonies were randomly selected. Crude periplasmic extracts were analyzed for the presence of specific antigens using ELISA. Forty-seven colonies were positive, and nucleotide sequencing revealed these represented 35 different nanobodies that belonged to 17 distinct groups based on sequence alignments. In this study, we examined two nanobodies (termed Nano-25 and Nano-85) that represented two distinct groups. The nanobodies were cloned into a pHEN6C expression vector and grown in WK6 cells overnight at 28°C. Expression was induced with 1 mM IPTG at an OD_{600} of 0.7 to 0.9. Nanobodies were extracted from periplasm and the supernatant collected. Nanobodies were eluted from a Ni-NTA column after a series of washing steps and purified by size-exclusion chromatography using a Superdex-200 column. Nanobodies were concentrated to 2 to 5 mg/ml and stored in GFB.

Nanobody reactivities using ELISA. The nanobody reactivities against norovirus VLPs and P domains were determined using a direct ELISA as previously described, with slight modifications (18), i.e., His tag nanobodies were detected with a secondary horseradish peroxidase (HRP)-conjugated anti-His IgG. Microtiter plates (Maxisorp, Denmark) first were coated with 100 μl (2 μg/ml) of VLPs (GII.10, GII.12, GII.4, and GI.1) or 100 μl (7 μg/ml) of GII.10 P domain in PBS (pH 7.4). Wells were washed three times with PBS (pH 7.4) containing 0.1% Tween 20 (PBS-T) and then blocked with 300 μl of PBS containing 5% skim milk (PBS-SM) for 1 h at room temperature. After washing, 100 μl of serially diluted nanobodies in PBS (from ~10 μM) were added to each well. The wells were washed, and then 100 μl of a 1:3,000 dilution of secondary HRP-conjugated anti-His IgG (Sigma) was added to wells for 1 h at 37°C. After washing, 100 μl of substrate *o*-phenylenediamine and H_2O_2 was added to wells and left in the dark for 30 min at room temperature. The reaction was stopped with the addition of 50 μl of 3N HCl, and the absorbance was

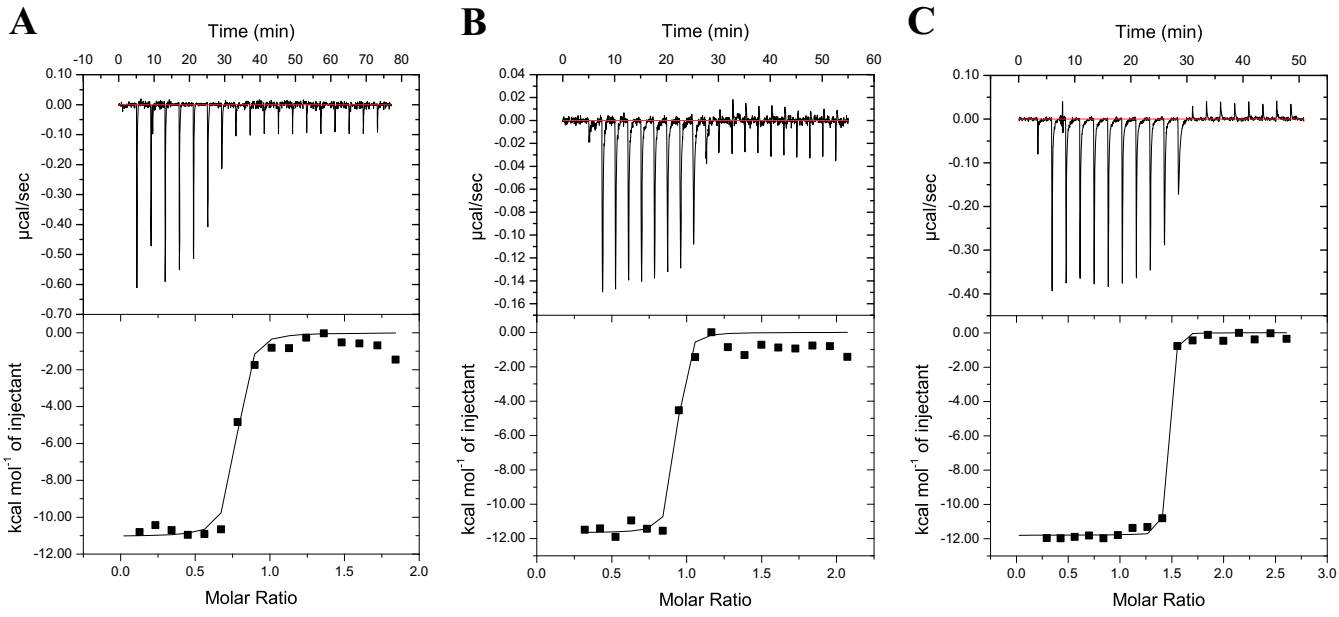

D

	GII.10 Nano-25		GII.10 Nano-85		GII.4 Nano-85	
	Av.	STD	Av.	STD	Av.	STD
K	2,77E-08	1,44E-08	7,00E-09	2,49E-10	3,47E-09	1,83E-09
dH	-1,14E+04	5,97E+02	-1,15E+04	5,07E+02	-1,17E+04	9,07E+01
dS	-3,61	1,48	-1,20	1,75	-0,36	1,12
dG	-1,04E+04	2,89E+02	-1,11E+04	1,67E+01	-1,16E+04	3,95E+02

FIG 4 Thermodynamic properties of nanobody binding to P domains. ITC experiments were performed using an ITC-200. Titrations were performed at 25°C by injecting consecutive (2 to 3 μl) aliquots of nanobodies (100 μM) into P domains (10 to 20 μM) in 120-s intervals. Examples of the titration (upper) of nanobodies to norovirus P domains are shown. (A) Nano-25 to GII.10 P domain; (B) Nano-85 to GII.10 P domain; (C) Nano-85 to NSW-2012 GII.4 P domain. The binding isotherm was calculated using a single binding site model (lower). (D) Constants *K* (binding constant in M^{-1}), d*H* (heat change in cal/mol), d*S* (entropy change in cal/mol/deg), and d*G* (change in free energy in cal/mol) are shown. Av., average; STD, standard deviations.

measured at 490 nm (OD_{490}). All experiments were performed in triplicate. The final OD_{490} is the $sample_{mean}$ minus the PBS_{mean} (i.e., ~0.05). A cutoff limit was set at an OD_{490} of >0.15, which was ~3 times the value of the negative control (PBS).

For the Nano-85 sandwich ELISA, plates first were coated overnight with 100 μl (~5 μM) of commercially available monoclonal antibodies. For GII.4 VLPs, we used 10E2 monoclonal antibody (ViroStat, USA), and for GII.10 and GII.12 VLPs, we used 4933 monoclonal antibody (ViroStat, USA). Wells were washed and then blocked for 1 h at room temperature. After washing, 100 μl (2 μg/ml) of VLPs (GII.10, GII.12, and GII.4) was added to each well for 1 h at 37°C. After washing, 100 μl of serially diluted Nano-85 in PBS (from ~10 μM) was added to each well. The plates were incubated for 1 h at 37°C and then processed as described above, with the cutoff limit set at an OD_{490} of >0.15.

Clinical screening using a sandwich ELISA. In order to determine the potential of Nano-85 as a detection reagent for clinical specimens, 30 stool specimens from patients presenting sporadic gastroenteritis were screened using a modified sandwich ELISA (18). Twelve specimens were determined as GII.4 norovirus positive using single-round reverse transcription-PCR (RT-PCR) (primers G2F3 and NV2oR) (19, 20) and sequence analysis (unpublished). Wells first were coated with 100 μl (~5 μM) of 10E2 monoclonal antibody for 2 h at 37°C. Wells were washed and then blocked for 2 h at room temperature. Stool specimens were thawed to room temperature, and a 10% stool suspension was prepared in PBS. The suspension was vortexed and centrifuged at 5,000 rpm for 5 min. After washing the wells, 100 μl of clarified stool supernatant was added to duplicate wells for 2 h at 37°C. Wells were washed, and then 100 μl of ~2.5 μM Nano-85 was added to wells. The plates were incubated for 1 h at 37°C and then processed as described above. An ELISA-positive reaction was determined at an OD_{490} of >0.2 (1), where the final sample OD_{490} was the $sample_{mean}$ minus the PBS_{mean} (i.e., ~ 0.11).

VLP detection limit using a sandwich ELISA. The detection limit of a sandwich ELISA was examined using purified VLPs spiked in a 10% norovirus-negative stool suspension as previously described (18). Briefly, plates first were coated with a 100-μl (~5 μM) mixture of 10E2 and 4933 monoclonal antibodies for 2 h at 37°C (i.e., 10E2 bound GII.4 VLPs and 4933 bound GII.10 VLPs). Wells were washed and then blocked for 2 h at room temperature. After washing, 100 μl (10 μg/ml) of GII.10 and GII.4 VLPs spiked separately in 10% stool suspensions was serially diluted in 10% stool suspension and added to duplicate wells for 2 h at room temperature and then detected as described above. An ELISA-positive reaction was determined at an OD_{490} of >0.2 (1), where the final sample OD_{490} was the sample OD_{490} minus the PBS_{mean} (i.e., ~0.15).

ITC measurements. Isothermal titration calorimetry (ITC) experiments were performed using an ITC-200 (GE Healthcare). Samples were prepared in GFB and filtered prior to experiments. Titrations were per-

TABLE 1 Data collection and refinement statistics of P domain Nanobody complex structures[a]

Parameter	GII.10 Nano-25 (4X7C)	GII.10 Nano-85 (4X7D)	GII.4 2006 Nano-85 (4X7E)	GII.4 2012 Nano-85 (4X7F)
Data collection				
Space group	$P2_12_12_1$	$P12_11$	$P22_12_1$	$P2_12_12_1$
Cell dimensions				
a, *b*, *c* (Å)	49.28, 112.98, 142.89	51.94, 133.1, 67.57	50.15, 125.23, 133.04	70.64, 93.58, 136.68
α, β, γ (°)	90, 90, 90	90, 112.54, 90	90, 90, 90	90, 90, 90
Resolution (Å)	46.59–1.69 (1.76–1.69)	47.97–2.11 (2.19–2.11)	46.93–1.98 (2.05–1.98)	46.79–2.15 (2.23–2.15)
R_{sym}	5.64 (40.54)	7.88 (47.95)	12.11 (76.77)	84 (65.33)
$I/\sigma(I)$	14.34 (2.09)	11.62 (2.09)	13.23 (2.47)	11.79 (2.02)
Completeness (%)	99.12 (95.09)	95.85 (93.14)	98.61 (87.81)	99.45 (98.79)
Redundancy	4.7 (3.6)	2.9 (2.9)	9.5 (8.8)	3.7 (3.8)
Refinement				
Resolution (Å)	46.59–1.70	47.97–2.11	46.9–2.0	46.79–2.15
No. of reflections	88,060	46,603	58,271	49,755
R_{work}/R_{free}	0.16/0.19	0.19/0.22	0.17/0.22	0.20/0.24
No. of atoms	6,921	6,774	6,908	6,792
Protein	6,349	6,448	6,480	6,365
Ligand/ion	108	36	0	8
Water	464	290	428	419
Average *B* factors (Å^2)				
Protein	32.60	35.80	34.80	39.90
Ligand/ion	42.20	43.50		32.10
Water	38.60	35.30	38.70	36.50
RMSD				
Bond lengths (Å)	0.011	0.005	0.009	0.012
Bond angles (°)	1.26	0.77	1.21	1.28

[a] Each data set was collected from single crystals. Values in parentheses are for the highest-resolution shell.

formed at 25°C by injecting consecutive (2 to 3 μl) aliquots of nanobodies (100 μM) into P domains (10 to 20 μM) in 120-s intervals. Injections were performed until saturation was achieved. To correct for heats of dilution from titrants, control experiments were performed by titrating nanobodies into GFB. The heat associated with the control titration was subtracted from raw binding data prior to fitting. The data were fitted using a single set-binding model (Origin 7.0 software). Nanobody binding sites were assumed to be identical.

Purification and crystallization of norovirus P domain and nanobody complexes. The P domain and nanobody were mixed at a 1:1.4 molar ratio and incubated at 25°C for ~90 min. The complex was purified by size-exclusion chromatography using a Superdex-200 column and concentrated to 2.8 mg/ml. Complex crystals were grown using a hanging-drop vapor diffusion method at 18°C for ~6 to 10 days. GII.10 P domain and Nano-85 crystals were grown in 0.2 M calcium acetate, 18% (wt/vol) polyethylene glycol (PEG) 8000, and 0.1 M sodium cacodylate (pH 6.5). GII.10 P domain and Nano-25 crystals were grown in 20% (wt/vol) PEG 3350 and 0.2 M ammonium dihydrogen phosphate. Saga-2006 GII.4 P domain and Nano-85 crystals were grown in 20% (wt/vol) PEG 3350, 0.2 M ammonium fluoride. NSW-2012 GII.4 P domain and Nano-85 crystals were grown in 10% (wt/vol) PEG 8000 and 0.1 M HEPES (pH 7.5). Prior to flash freezing in liquid nitrogen, crystals were transferred to a cryoprotectant containing the mother liquor in 30% ethylene glycol.

GII.10 VLP Nano-85 complex purification. In order to better understand how Nano-85 might bind to intact VLPs, we purified a GII.10 VLP Nano-85 complex from a Ni-NTA column using the nanobody His tag. Briefly, the GII.10 VLPs (10 mg/ml) and Nano-85 (3.4 mg/ml) were mixed (1:3 molar ratio) and incubated for 1 h at room temperature. The GII.10 VLP Nano-85 mixture was preincubated with Ni-NTA and added to the column. After a series of washing steps (10, 20, and 50 mM imidazole in Tris-HCl-NaCl), the GII.10 VLP Nano-85 complex was eluted from the column with 250 mM imidazole in Tris-HCl-NaCl and examined using SDS-PAGE, a sandwich ELISA, and EM. For a negative control, GII.10 VLPs only were processed as described above, and all fractions were collected and examined using SDS-PAGE and ELISA. For this sandwich ELISA, plates first were coated overnight with 100 μl (1:10,000 dilution) of GII.10 VLP-specific polyclonal rabbit serum (termed GII.10-VLP-rabbit-1). Wells were washed and then blocked for 1 h at room temperature. The VLP Nano-85 complex, VLPs only (negative control), and Nano-85 (negative control) were serially diluted and added to each well (triplicates). After washing, the wells were detected with the secondary HRP-conjugated anti-His IgG as described earlier.

Data collection, structure solution, and refinement. X-ray diffraction data were collected at the European Synchrotron Radiation Facility, France, at beamlines BM30A and ID23-1 and processed with XDS (21). Structures were solved by molecular replacement in PHASER (22). The GII.10 P domain was solved using molecular replacement with GII.10 P domain (3ONU) and a previously determined nanobody (3P0G) as search models. Structures were refined in multiple rounds of manual model building in COOT (23) and refined with PHENIX (24). Structures were validated with Procheck (25) and Molprobity (26). PISA software was used to determine binding interfaces and calculate surface area (27). Binding interactions were analyzed using Accelrys Discovery Studio (version 4.1), with hydrogen bonding interactions distances between 2.4 and 3.5Å and hydrophobic interaction distances between 3.4 and 4.5Å. Figures and protein contact potentials were generated using PyMOL (version 1.12r3pre).

Protein structure accession number. Atomic coordinate and structure factors of the X-ray crystal structures were deposited in the Protein Data Bank under accession numbers 4X7C, 4X7D, 4X7E, and 4X7F.

RESULTS

Nanobody binding specificity using ELISA. The two nanobodies investigated in this study, Nano-85 and Nano-25, were raised against GII.10 VLPs in a single alpaca. Nano-85 and Nano-25 had 70% amino acid identity and were considered uniquely different (Fig. 1). Initially, the nanobody binding characteristics were analyzed with the GII.10 VLPs and the corresponding GII.10 P do-

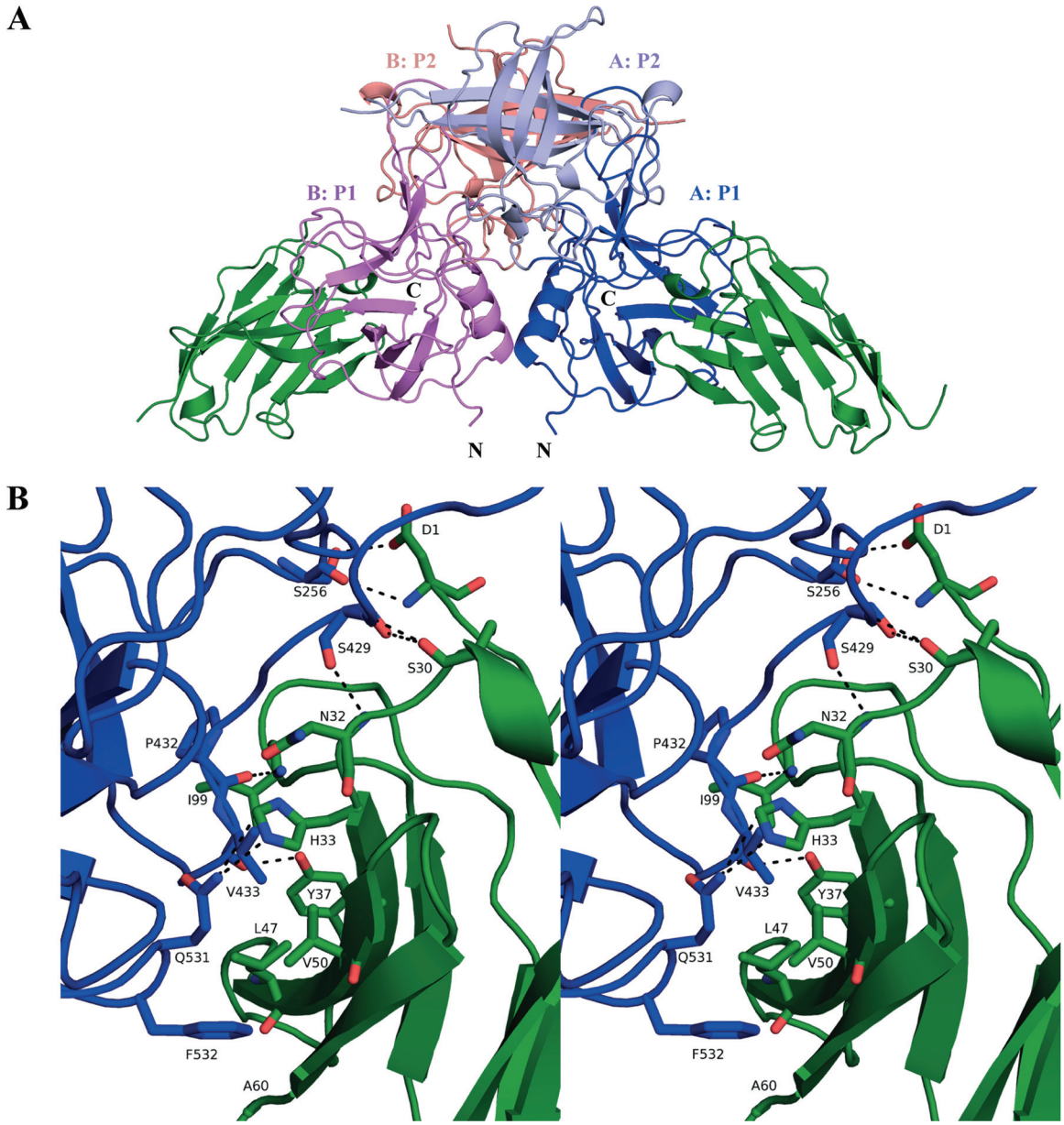

FIG 5 Structure of GII.10 domain Nano-25 complex. (A) The X-ray crystal structure of the GII.10 domain Nano-25 complex was determined to 1.70-Å resolution. The complex was colored according to GII.10 P domain monomers (chains A and B) and P1 and P2 subdomains, i.e., chain A, P1 (blue); chain A, P2 (light blue); chain B, P1 (violet); chain B, P2 (salmon); and Nano-25 (green). Nano-25 bound to the lower region of the P1 subdomain and involved a monomeric interaction. (B) A closeup stereo view of (chain A) GII.10 P domain- and Nano-25-interacting residues. The GII.10 P domain hydrogen bond interactions involved both side-chain and main-chain interactions (bond length of 2.8 to 3.3 Å), one side chain and one main chain of S256, two main chains and one side chain of S429, one main chain of P432, one main chain of V433, and one side chain of Q531. GII.10 P domain hydrophobic interactions (3.6 to 5.1 Å) involved P432, V433, and F532.

main using a direct ELISA. Plates first were coated with VLPs or P domains. After washing and blocking steps, serially diluted nanobodies were added to each well. The nanobodies subsequently were detected using a secondary antibody. Nano-85 detected GII.10 VLPs at a dilution of 64,000 (~170 pM), whereas Nano-25 detected GII.10 VLPs at a lower dilution of 16,000 (Fig. 2A). A similar binding pattern was observed with the GII.10 P domain, where Nano-85 and Nano-25 detected the GII.10 P domains at dilutions of 17,280 and 2,160, respectively (Fig. 2B).

The nanobody cross-reactivities were analyzed with GI.1, GII.4 (NSW-2012), and GII.12 VLPs using a similar ELISA. Nano-85 detected GII.4 and GII.12 VLPs at dilutions of 69,120 and 34,560, respectively (Fig. 2C). Nano-85 cross-reacted weakly against GI.1 VLPs, i.e., at a dilution of less than 4,000 (data not shown). Nano-25 did not cross-react against GI.1, GII.4, and GII.12 VLPs (data not shown). These results indicated that Nano-85 was broadly reactive, whereas Nano-25 was specific for GII.10.

In order to confirm Nano-85 cross-reactivity and binding to intact particles, a sandwich ELISA was performed. Plates first were coated with capture monoclonal antibodies. After washing and

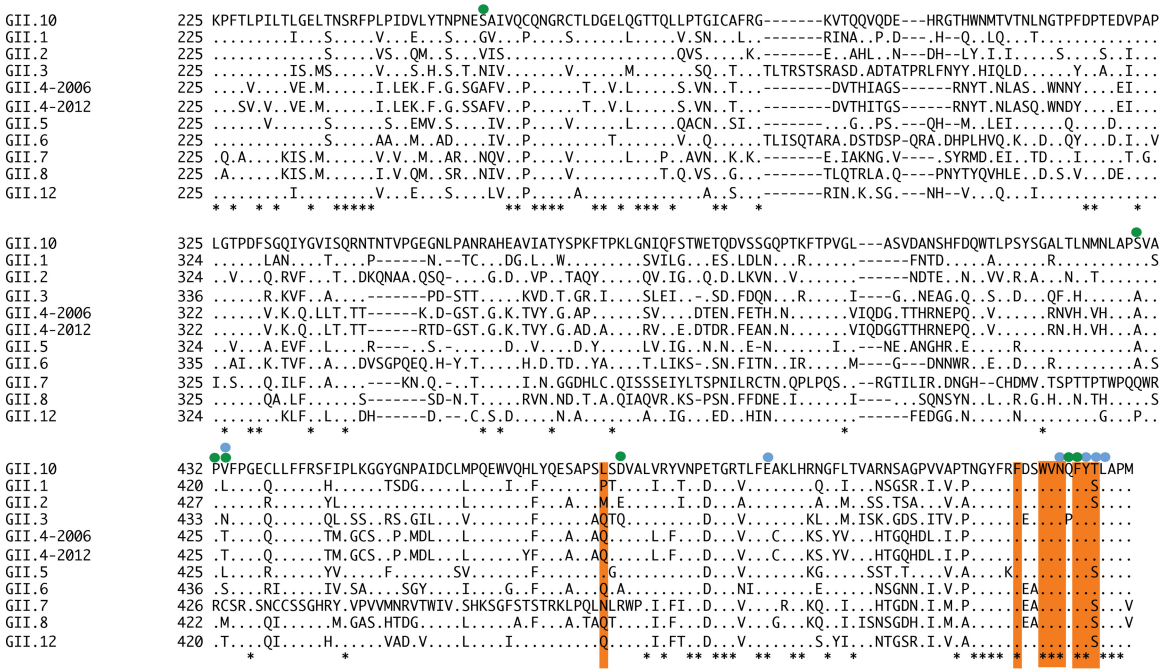

FIG 6 Amino acid alignment of GII P domain sequences. Eleven GII genotype sequences (P domain shown) were aligned using ClustalX. The GII.10 capsid sequence (AF504671) was used as the consensus, along with GII.1 (U07611), GII.2 (HCU75682), GII.3 (DQ093066), Saga-2006 GII.4 (AB447457), NSW-2012 GII.4 (JX459908), GII.5 (BD011877), GII.6 (DQ093064), GII.7 (BD011881), GII.8 (AB039780), GII.10, and GII.12 (AB044366). The GII.10 amino acids interacting with Nano-25 (green circles), Nano-85 (orange), and 5B18 Fab (blue circles) were marked accordingly. The asterisks indicate conserved amino acids.

blocking steps, GII.4, GII.10, and GII.12 VLPs were added to wells. After washing, serially diluted Nano-85 was added to each well. Nano-85 subsequently was detected using the secondary antibody. Nano-85 detected GII.10, GII.12, and GII.4 VLPs at dilutions of 17,280, 8,640, and 2,160, respectively (Fig. 2D). The sandwich ELISA results confirmed that Nano-85 was broadly reactive and likely bound to intact particles.

Clinical testing and detection limit of Nano-85 using ELISA. The diagnostic potential of Nano-85 was evaluated using a sandwich ELISA and clinical stool specimens from patients with sporadic gastroenteritis. A total of 12 GII.4 norovirus-positive and 18 GII.4-negative specimens were screened. A positive reaction was considered to occur at an OD_{490} of >0.2. The ELISA detected 4 of 12 RT-PCR-positive specimens, where the OD_{490} ranged between 0.43 and 0.78 (Fig. 3A). One GII.4 RT-PCR-negative specimen (number 48) had an OD_{490} of 0.38, which suggested an ELISA false-positive result. Taken together, these ELISA data indicated that Nano-85 could work as a reagent in a diagnostic ELISA kit, although further testing and modifications would be required.

The detection limit of a sandwich ELISA and confirmation that Nano-85 detected norovirus particles was examined using purified GII.10 and GII.4 VLPs spiked separately in a 10% norovirus-negative stool suspension. A positive reaction was considered to occur at an OD_{490} of >0.2. Nano-85 was capable of detecting ~5 μg/ml and ~0.3 μg/ml of GII.4 and GII.10 VLPs, respectively (Fig. 3B). These results confirmed that Nano-85 bound norovirus particles and indicated that the stool suspension does not inhibit the ELISA.

Thermodynamic properties of nanobody binding to P domains. The thermodynamic properties of Nano-85 and Nano-25 binding to GII.10, GII.4 (NSW-2012), and GII.12 P domains were evaluated using ITC (Fig. 4). The titration of nanobodies to the P domains showed a specific binding and formation of complexes with an exothermic heat of binding (Fig. 4A, B, and C, upper). The binding isotherm, which is an increment of heat release as a function of complex formation, was calculated using a single binding site model (Fig. 4A, B, and C, lower). The resulting binding constants are shown in Fig. 4D. The nanobodies tightly bound to the P domains (GII.10 P domain and Nano-25, dissociation constant [K_d] of 28 nM; GII.10 P domain and Nano-85, K_d of 7 nM; GII.4 P domain and Nano-85, K_d of 3.5 nM). The interactions were largely enthalpy driven, which suggested the net formation of noncovalent bonds was a major contributor to the affinity.

X-ray structures of norovirus P domain and nanobody complexes. In order to identify the nanobody recognition sites, we determined the X-ray crystal structures of GII.10 P domain in complex with Nano-25 and Nano-85. We also determined the X-ray crystal structures of two variant GII.4 P domains (Saga-2006 and NSW-2012) in complex with Nano-85 in order to better understand cross-reactivity interactions at the atomic resolution. The P domain-nanobody complexes were purified using size exclusion chromatography. The complexes were crystallized and X-ray diffraction data were collected. Data statistics for the P domain nanobody complex structures are shown in Table 1.

The GII.10 P1 subdomain was comprised of residues 222 to 277 and 427 to 549, whereas the P2 subdomain was located between residues 278 and 426 (17). The GII.4 P1 subdomains were comprised of residues 224 to 274 and 418 to 530, whereas the P2 subdomains were located between residues 275 and 417 (42). The P1 subdomains contained the typical β-sheets and one α-helix, whereas the P2 subdomains contained six antiparallel β-strands that formed a barrel-like structure. The P domains in the complexes were reminiscent of

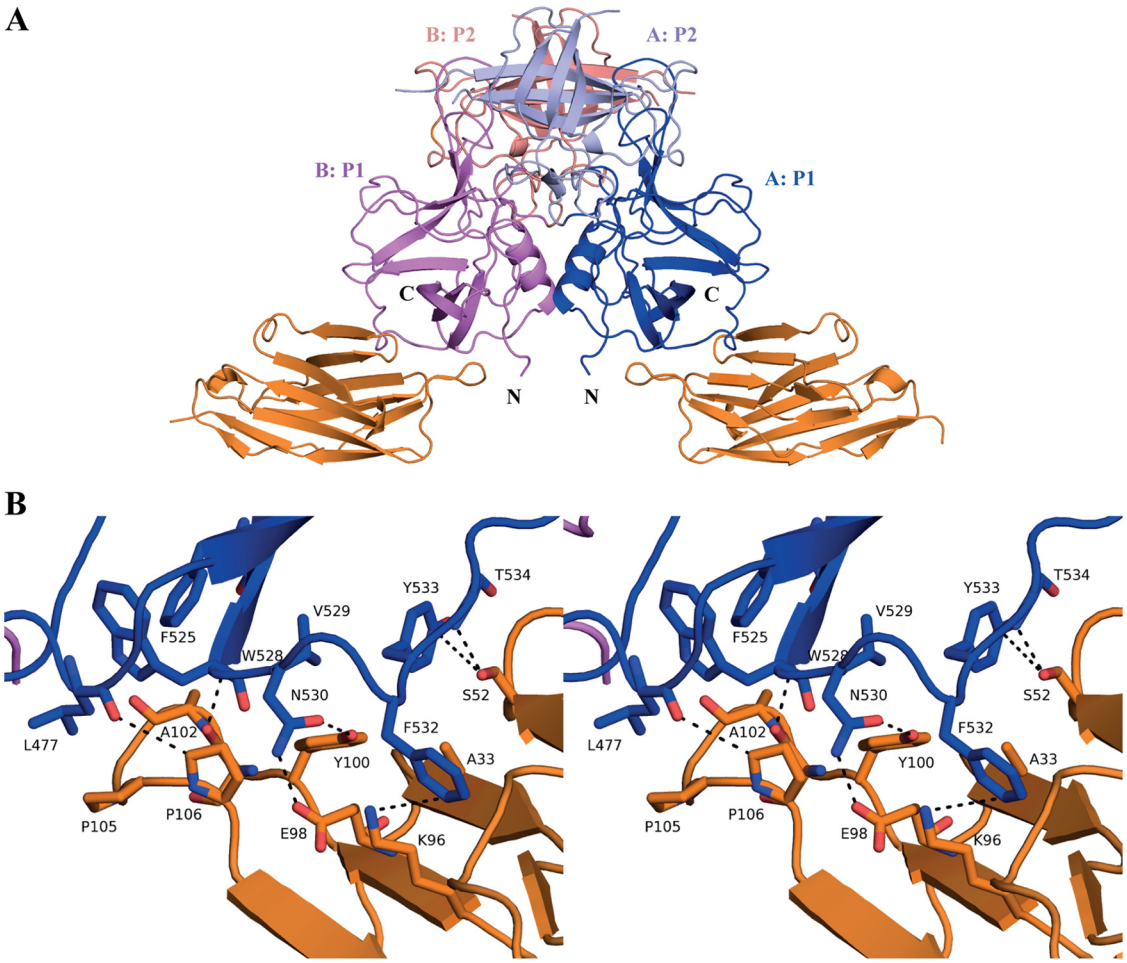

FIG 7 Structure of GII.10 domain Nano-85 complex. (A) The X-ray crystal structure of the GII.10 domain Nano-85 complex was determined to 2.11-Å resolution. The complex was colored according to Fig. 2, with the exception of Nano-85 (orange). Nano-85 bound to the lower region of the P1 subdomain and involved a monomeric interaction. (B) A closeup stereo view of (chain A) GII.10 P domain- and Nano-85-interacting residues. The P domain hydrogen bond interactions included side-chain and main-chain interactions, one main chain of W528, two side chains of N530, and one main chain of T534. Two additional P domain interactions with Nano-85 were observed, F532, forming a hydrogen bond/electrostatic interaction, and Y533, forming a π donor hydrogen bond. P domain hydrophobic interactions involved L477, F525, V529, and F532.

the unbound P domains and showed little conformational change upon nanobody binding. Nano-25 and Nano-85 structures were well refined for most residues and showed a typical immunoglobulin domain fold of other known nanobody structures (28, 29). As expected, amino acid changes were located mostly in CDR-1, CDR-2, and CDR-3 (Fig. 1). Nano-85 CDR-3 contained a seven-amino-acid insertion compared to Nano-25 CDR-3.

Structure of GII.10 P domain Nano-25 complex. A single crystal of the GII.10 P domain Nano-25 complex diffracted to 1.69-Å resolution. The structure was solved using molecular replacement with GII.10 P domain (3ONU) and a sequence-related nanobody (3P0G) as search models. Molecular replacement indicated one P dimer and two Nano-25 molecules in space group $P2_12_12_1$. Five possible binding interfaces derived from the crystal packing were detected using an online server (PISA). Four binding interfaces had a small surface area (<438 Å^2) and Nano-25 had few interacting residues, all of which were located outside the CDRs (see Fig. S1 in the supplemental material). One interface had a large surface area (866 Å^2) and involved a network of hydrogen bonds and hydrophobic interactions (Fig. 5). In addition, the Nano-25 interacting residues at this interface were located mainly in the three CDRs (Fig. 1). Therefore, these results indicated that the biologically relevant interface was at this location, which was at the lower region of the P1 subdomain and involved a monomeric interaction (Fig. 5).

Five P domain residues (Ser256, Ser429, Val433, Pro432, and Gln531) formed nine direct hydrogen bonds with Nano-25. Three P domain residues (Pro432, Val433, and Phe532) were involved in six hydrophobic interactions with Nano-25. One salt bridge between Asp479 of the P domain and Nano-25 was observed. A similar set of binding interactions also was observed with the second Nano-25 molecule (data not shown).

An amino acid sequence alignment of representative GII P domains showed that the six P domain residues (Ser256, Ser429, Pro432, Val433, Asp479, and Gln531) interacting with Nano-25 were mainly variable (Fig. 6). This result corresponded well with the ELISA data that showed Nano-25 was GII.10 specific.

Structure of GII.10 P domain Nano-85 complex. The GII.10 P domain Nano-85 complex diffracted to 2.11-Å resolution. Molecular replacement indicated one P dimer and two Nano-85 mole-

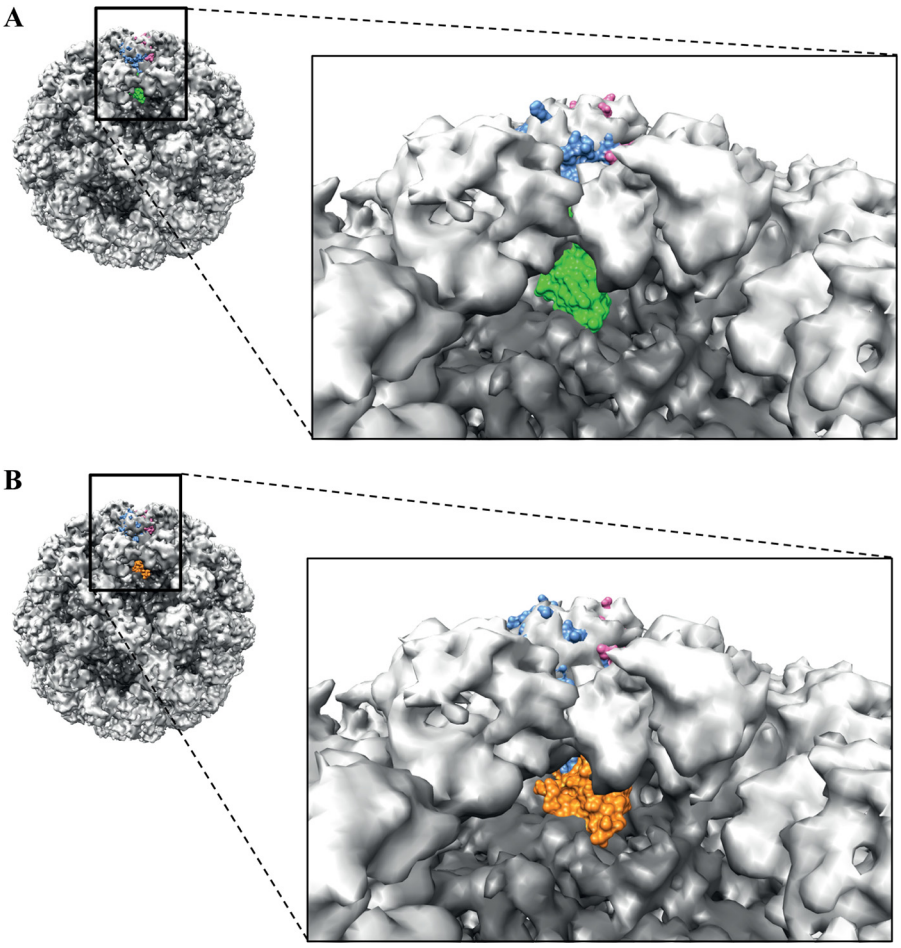

FIG 8 X-ray crystal structure of the GII.10 P domain Nano-25 complex and GII.10 P domain Nano-85 complex fitted into the cryo-EM GII.10 VLP structure. The cryo-EM VLP structure was colored according to S (dark gray) and P domains (light gray). The P dimer (light blue and pink) from the P domain nanobody complexes was manually fitted into the P dimer on the VLP. (A) The P domain Nano-25 complex fitted on the VLP, showing the position of Nano-25 (green) in the context of the particle. The boxed region shows a close-up view of the complex. Nano-25 clashed with neighboring P domains on the VLP and rested on top of the S domain. (B) The P domain Nano-85 complex fitted on the VLP, showing the position of Nano-85 (orange) in the context of the particle. The boxed region shows a close-up view of the complex. Nano-85 clashed with the neighboring P domains on the particle and rested on top of the S domain.

cules in space group $P12_11$ (Table 1). Crystal packing showed five possible Nano-85 binding interfaces on the P dimer. Four interfaces had surface areas of less than 388 Å^2 and few Nano-85 interacting residues, which were located outside the CDRs (see Fig. S1 in the supplemental material). One interface had a surface area of 736 Å^2 and contained numerous Nano-85-interacting residues from the three CDRs (Fig. 1). Based on these findings, the biologically relevant interface was considered to be at this site, which was on the lower region of the P1 subdomain and involved a monomeric interaction (Fig. 7).

The binding interaction between GII.10 P domain and Nano-85 mainly consisted of hydrogen bonds and hydrophobic interactions (Fig. 7B). Three P domain residues (Trp528, Asn530, and Thr534) formed four direct hydrogen bonds with Nano-85. Four P domain residues (Leu477, Phe525, Val529, and Phe532) formed five hydrophobic interactions with Nano-85. Additionally, we observed one electrostatic interaction between Phe532 of the P domain and Nano-85 and one π donor hydrogen bond between Tyr533 of the P domain and Nano-85. A similar set of binding interactions with the second Nano-85 molecule was observed on the other P domain monomer (data not shown).

A sequence alignment of GII P domains showed that seven GII.10 P domain residues (Phe525, Trp528, Val529, Asn530, Phe532, Tyr533, and Thr534) interacting with Nano-85 were mainly conserved (Fig. 6). This result suggested that Nano-85 was capable of binding broadly distinct GII genotypes, which was observed earlier using ELISA with GII.4 and GII.12 VLPs (Fig. 2).

Structure of Saga-2006 GII.4 P domain Nano-85 complex. Our ELISA data showed that Nano-85 was capable of binding GII.4 VLPs. However, the sequence alignment indicated that one GII.10 P domain amino acid (Leu477) interacting with Nano-85 was variable (GII.4 equivalent Gln469), and the variable amino acids nearby may affect the binding interactions (Fig. 6). Therefore, in order to better understand Nano-85 cross-reactivities at the atomic resolution, we solved the X-ray crystal structures of two GII.4 P domains (Saga-2006 and NSW-2012) in complex with Nano-85. Saga-2006 and NSW-2012 P domains shared 93% amino acid identity and ~55% amino acid identity with the GII.10 P domain (Fig. 6).

A single crystal of the Saga-2006 P domain Nano-85 complex diffracted to 1.98-Å resolution (Table 1). The favorable interface, similar to GII.10 P domain Nano-85 complex, had a surface area

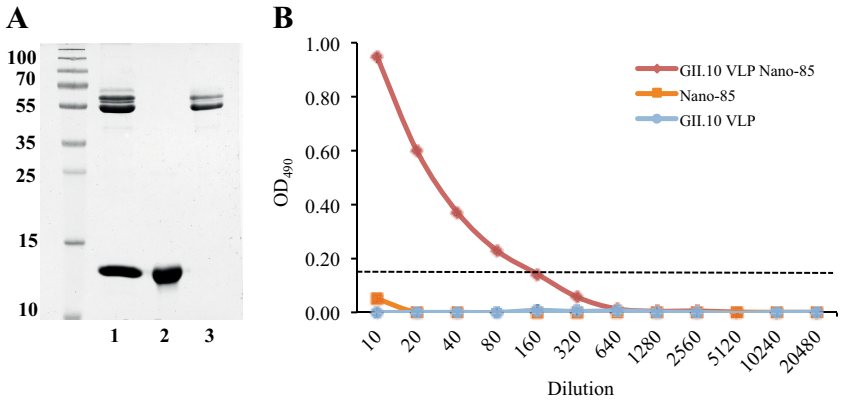

FIG 9 Analysis of VLP Nano-85 complex. (A) The GII.10 VLP Nano-85 complex was purified from a Ni-NTA column and examined using SDS-PAGE. Lane 1 showed the GII.10 VLP Nano-85-eluted fraction, lane 2 showed Nano-85 (positive control), and lane 3 showed GII.10 VLP (positive control). (B) GII.10-specific polyclonal antibody was coated on the plates. Serially diluted GII.10 VLP Nano-85 complex, GII.10 VLPs only, and Nano-85 only (negative control) were added to each well and then detected with a secondary HRP-conjugated anti-His IgG. The GII.10 VLP Nano-85 complex was detected in this ELISA format, whereas neither VLPs only nor Nano-85 only was detected.

of ~764 Å^2 and a network of binding interactions (see Fig. S2 in the supplemental material). Three P domain residues (Trp520, Asn522, and Thr526) formed four direct hydrogen bonds with Nano-85. Two P domain residues (Phe524 and Val521) formed three hydrophobic interactions with Nano-85. Unlike Leu477 of GII.10 P domain, which formed a hydrophobic interaction with Nano-85, the equivalent Gln469 of Saga-2006 GII.4 P domain did not form such an interaction. One π donor hydrogen bond interaction was formed between Tyr525 of the P domain and Nano-85.

Structure of NSW-2012 GII.4 P domain Nano-85 complex. A crystal of the NSW-2012 GII.4 P domain Nano-85 complex diffracted to 2.15-Å resolution (Table 1). Similar to the other Nano-85 complexes, the biologically relevant interface was found at the lower region of the NSW-2012 P1 subdomain (see Fig. S3A in the supplemental material). One of the Nano-85 molecules had higher-than-average B factors (~70 Å^2) and poor electron density on several loops that were not directly interacting with the P dimer (data not shown). NSW-2012 GII.4 P domain Nano-85 complex had a set of hydrogen bonds, hydrophobic interactions, and a π donor hydrogen bond that was similar to that of Saga-2006 GII.4 P domain Nano-85 complex (see Fig. S3B). Also, Gln469 of NSW-2012 GII.4 P domain (the equivalent to Leu477 of GII.10) did not form a hydrophobic interaction with Nano-85.

Superposition of the GII.10 P domain nanobody complex on the GII.10 VLP structure. The binding sites of both Nano-85 and Nano-25 were located on the lower region of the P1 subdomain. In order to better understand the nanobody binding in the context of the intact particles, the X-ray crystal structures of the GII.10 P domain Nano-25/Nano-85 complexes were manually positioned in the cryo-EM structure of the GII.10 VLP as previously described (11). The P dimers of the nanobody complexes unambiguously fit into the cryo-EM P dimer density map. However, the nanobodies had an obvious clash with neighboring P domains (Fig. 8). A similar situation was observed with the X-ray crystal structure of GII.10 P domain 5B18 Fab complex, where the Fab clashed with the neighboring P domains (11). Taken together, these results further underscored the possibility that the P domains on intact particles were capable of movement in order to accommodate nanobodies and antibodies.

Nano-85 binding interaction with intact VLPs. The ELISA indicated that Nano-85 bound to intact norovirus VLPs and virions (Fig. 2 and 3). The X-ray crystal structure GII.10 P domain Nano-85 complex showed the binding site on the lower region of the P domain (Fig. 7A). Superposition of the GII.10 P domain Nano-85 complex structure on the cryo-EM structure of the intact particle created a paradox, i.e., the Nano-85 binding site appeared occluded on intact particles (Fig. 8B).

In order to better understand how Nano-85 might bind to intact VLPs, we proceeded to purify a GII.10 VLP Nano-85 complex from a Ni-NTA column. After a series of washing steps, the VLP Nano-85 complex was eluted from the column and examined using SDS-PAGE, a sandwich ELISA, and EM. SDS-PAGE showed that VLPs and Nano-85 were eluted from the same fraction, which suggested that the VLPs bound Nano-85 (Fig. 9A). When VLPs only were purified from an equivalent Ni-NTA column, only the first wash fraction (10 mM imidazole) contained a VLP band (data not shown), indicating that VLPs only did not bind to the Ni-NTA column. The sandwich ELISA also was able to detected the VLP Nano-85 complex, whereas the VLP-only fraction and Nano-85 only showed no signals (Fig. 9B). Taken together, these results demonstrated that a VLP Nano-85 complex was formed, and this could be purified from a Ni-NTA column. To our surprise, we were not able to observe any VLPs in the VLP Nano-85 complex using EM (data not shown). Initially, we assumed the Ni-NTA elution buffer caused the VLPs in the complex to disassemble. However, when the VLPs were directly treated with the elution buffer, we still could observe intact VLPs (Fig. 10A). Therefore, we suspected that the Nano-85 binding interaction caused the VLPs in the complex to disassemble.

To explore this hypothesis, we examined the effects of a nonbinding GII.10 nanobody (Nano-21; unpublished data) with GII.10 VLP. To maintain identical buffer conditions, Nano-21 and Nano-85 first were dialyzed in PBS (pH 7.4) overnight at 4°C. The GII.10 VLPs then were incubated with either Nano-21 or Nano-85 at a ~1:1 molar ratio for 1 to 2 h at room temperature and examined using EM. Intact GII.10 VLPs were observed in the GII.10 VLP and Nano-21 mixture (Fig. 10B) but not in the GII.10 VLP and Nano-85 mixture (Fig. 10C). A similar situation occurred with a GII.4 NSW-2012 VLP and Nano-85 mixture

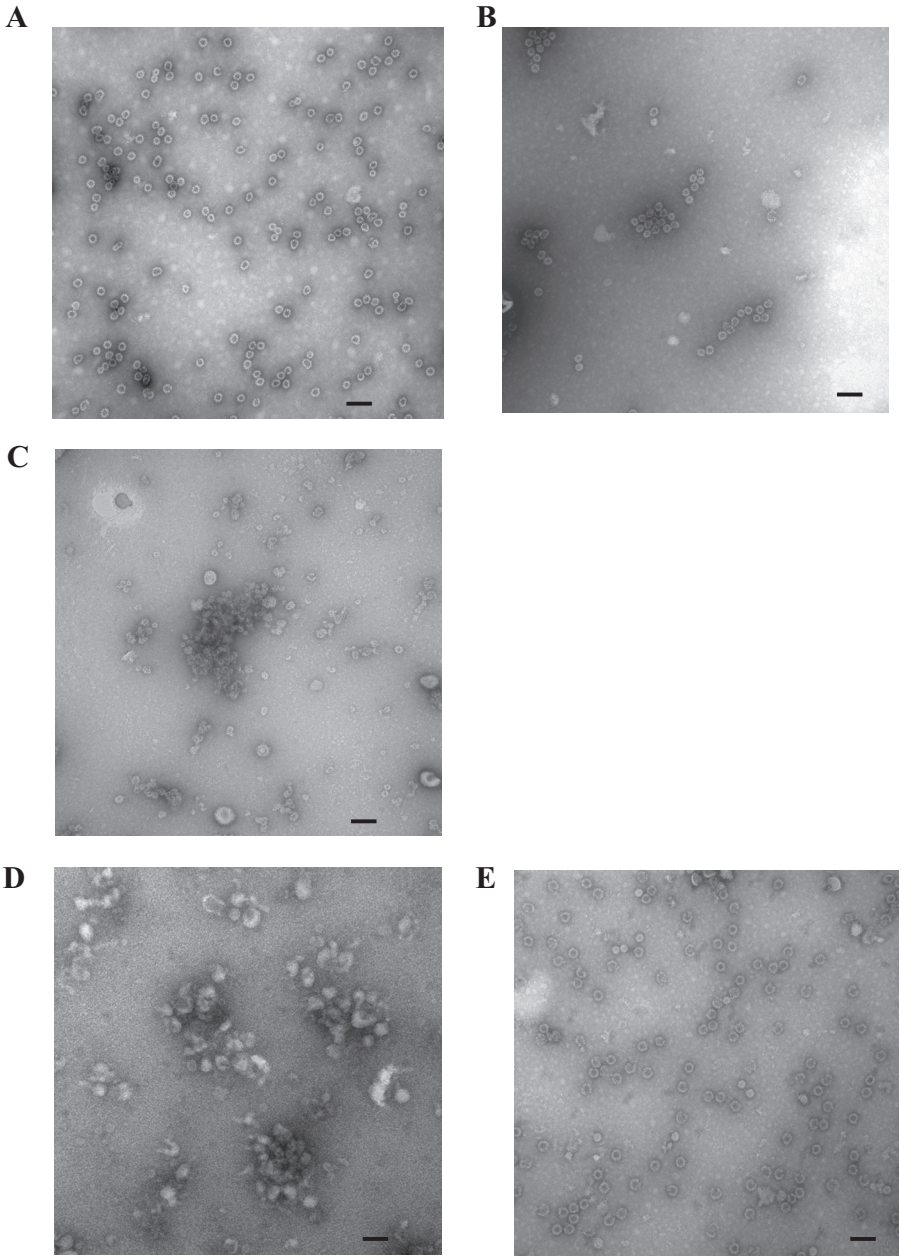

FIG 10 EM analysis of VLP nanobody complexes. Samples were applied to EM grids and stained with 4% uranyl acetate. (A) GII.10 VLP treated with elution buffer (250 mM imidazole in Tris-HCl-NaCl), (B) GII.10 VLP and Nano-21 mixture, (C) GII.10 VLP and Nano-85 mixture, (D) NSW-2012 GII.4 VLP and Nano-85 mixture, and (E) NSW-2012 GII.4 VLP treated with elution buffer. The scale bar represents ~100 nm.

(Fig. 10D and E). These results showed that Nano-85 binding to intact VLPs caused the particles to disassemble, while addition of the nonbinding Nano-21 had no effect on the VLPs.

DISCUSSION

In this study, we continued our structural investigations on functional norovirus epitopes using nanobodies. We sought to discover broadly reactive nanobodies and describe their binding interactions on the norovirus P domains. Nanobodies are gaining a lot of interest in diagnostics, therapeutics, and basic research. They have been used for virus detection of HIV (30, 31), vaccinia virus (32), Marburg virus (33), and Dengue virus (34). Nanobodies were shown to block virus attachment to cellular receptors in HIV and influenza virus (35–37). They also have been evaluated in phase I and II clinical trials in other areas, including oncology, neurology, and immunology (38). Compared to other recombinant antibody fragments (e.g., Fab and scFv), nanobodies benefit from superior intrinsic biophysical properties, such as high refolding efficiency, high solubility, resistance to proteases and chemical denaturants, and high expression levels.

Nanobodies have not yet been utilized, to the best of our knowledge, in norovirus detection systems. Both nanobodies had high affinities to norovirus particles; however, Nano-25 was GII.10 specific, whereas Nano-85 detected antigentically distinct

VLPs, including GII.4, GII.10, and GII.12 (amino acid identity, 58 to 93%). Our results showed that Nano-85 could detect the current pandemic GII.4 norovirus virions in clinical stool specimens from patients with sporadic gastroenteritis using a sandwich ELISA format, although the detection rate was low. On the other hand, most ELISA detection kits currently are used for screening outbreak specimens and have low detection rates with sporadic specimens (18, 39–41). Therefore, these results showed that Nano-85 might function as a valuable reagent in a diagnostic detection kit, although we acknowledge that additional ELISA formats will need to be tested in order to improve the detection rate.

Functional norovirus capsid epitopes still are poorly understood. There are currently only three high-resolution structures of norovirus particles (9–11), and little is known about antibody binding interactions with intact particles. Our structural analysis indicated that Nano-85 and Nano-25 P1 subdomain binding sites were occluded on intact particles (Fig. 8). We previously showed that 5B18 Fab bound at a region similar to that of Nano-85 on the P1 subdomain, which was occluded on intact particles (11). Other monoclonal antibodies, MAb14-1, NV3901, and NV3912, also were reported to bind at the lower region of the P1 subdomain, although structural data are lacking (13, 14).

A sequence alignment of representative GII genotypes indicated that Nano-85 interacted with five highly conserved residues (Phe525, Val529, Asn530, Phe532, and Tyr533) and two moderately conserved residues (Leu477 and Thr534) on the P domains (Fig. 6). Likewise, the 5B18 Fab interacted with four highly conserved residues (Glu500, Asn530, Tyr533, and Lys535) and two moderately conserved residues (Val433 and Thr534) on the P1 subdomain (Fig. 6). Interestingly, Nano-85 and these monoclonal antibodies (5B18, MAb14-1, and NV3901/NV3912) all were raised against different norovirus VLPs. Nano-85 was raised against GII.10 (Vietnam026 strain), 5B18 was raised against GII.4 (445 strain), MAb14-1 was raised against GII.4 (1207 strain), and NV3901/NV3912 were raised against GI.1 (NV strain). These data suggested that the lower region of the P1 subdomain (residues ~523 to 534) contained important and possibly dominant epitopes. Moreover, many of these antibodies currently are used in diagnostic ELISA kits for detecting norovirus virions in stool specimens. Consequently, the P1 subdomain nanobody/antibody binding region likely was accessible on intact particles, although in the context of the intact particle the binding sites were occluded.

Norovirus P domains are connected to the S domain via a "flexible" hinge region. The hinge region, ~10 to 12 amino acids long, is mostly conserved among different GII genotypes (1). The X-ray structure of the GI.1 VLPs showed that the hinge region contained no secondary structure features. The cryo-EM structure of GII.10 VLPs showed the P domain was raised off the S domain by ~15 Å. Subsequently, these findings suggested that the P domains on the particles could be flexible (11, 12). Moreover, we assumed that the P domains were able to move on the S domain in order to accommodate Nano-85, Nano-25, and 5B18 monoclonal antibody, since there was an apparent clash with neighboring P domains on the VLP structure (Fig. 8). Unfortunately, there is still no direct evidence that these nanobodies or antibody bound to intact particles apart from sandwich ELISA data.

The most convincing evidence that these nanobodies bound intact VLPs would be a VLP nanobody complex structure. Unfortunately, our attempts to purify intact VLP Nano-85 complexes failed. Instead, we discovered that Nano-85 binding caused VLP disassembly. This result was somewhat unexpected, since intact VLPs were observed when VLPs were mixed with 5B18 IgG (11). Moreover, three P1 subdomain residues (Asn530, Tyr533, and Thr534) interacted with both 5B18 monoclonal antibody and Nano-85 (Fig. 6). This finding suggested that the P domain residues interacting with Nano-85 represented an essential epitope and trigger region for particle disassembly. Interestingly, Nano-85 contained an extended CDR-3 loop that appeared to lodge itself between the S and P domains, suggesting that Nano-85 could have operated as a kind of fulcrum in the particle disassembly process. It is tempting to speculate that this particle disassembly process is analogous to virion disassembly *in vivo*. On the other hand, a vulnerable trigger region may need to be concealed and occluded from the host defenses. Further studies are needed to investigate these notions.

In summary, these new discoveries have identified a highly conserved epitope that could represent a potential site of norovirus vulnerability. We remain optimistic that, with further testing, Nano-85 will not only work as a diagnostic reagent but also function as a broadly reactive GII norovirus antiviral.

ACKNOWLEDGMENTS

Funding for this study was provided by the CHS foundation and the Helmholtz-Chinese Academy of Sciences.

We acknowledge the European Synchrotron Radiation Facility (ID23-1, ID30A, and BM30A) for provision of synchrotron radiation facilities. We are grateful to Vesna Blazevic and Suvi Lappalainen for supplying the NSW-2012 and NV bacmid constructs, Paul Schnitzler and Julia Tabatabai for the clinical specimens, Doug McAllister (ViroStat Inc., USA) for the monoclonal antibodies, and Anja Drescher and Thomas Keck for the use of the ITC-200 machine.

A patent for Nano-85 is pending (A. D. Koromyslova and G. S. Hansman, application number EP14188878.4).

REFERENCES

1. **Hansman GS, Natori K, Shirato-Horikoshi H, Ogawa S, Oka T, Katayama K, Tanaka T, Miyoshi T, Sakae K, Kobayashi S, Shinohara M, Uchida K, Sakurai N, Shinozaki K, Okada M, Seto Y, Kamata K, Nagata N, Tanaka K, Miyamura T, Takeda N.** 2006. Genetic and antigenic diversity among noroviruses. J Gen Virol **87:**909–919. http://dx.doi.org/10.1099/vir.0.81532-0.
2. **Vinje J.** 2 July 2014. Advances in laboratory methods for detection and typing of norovirus. J Clin Microbiol http://dx.doi.org/10.1128/JCM.01535-14.
3. **Kroneman A, Vega E, Vennema H, Vinje J, White PA, Hansman G, Green K, Martella V, Katayama K, Koopmans M.** 2013. Proposal for a unified norovirus nomenclature and genotyping. Arch Virol **158:**2059–2068. http://dx.doi.org/10.1007/s00705-013-1708-5.
4. **Siebenga JJ, Vennema H, Renckens B, de Bruin E, van der Veer B, Siezen RJ, Koopmans M.** 2007. Epochal evolution of GGII.4 norovirus capsid proteins from 1995 to 2006. J Virol **81:**9932–9941. http://dx.doi.org/10.1128/JVI.00674-07.
5. **Debbink K, Lindesmith LC, Donaldson EF, Costantini V, Beltramello M, Corti D, Swanstrom J, Lanzavecchia A, Vinje J, Baric RS.** 2013. Emergence of new pandemic GII.4 Sydney norovirus strain correlates with escape from herd immunity. J Infect Dis **208:**1877–1887. http://dx.doi.org/10.1093/infdis/jit370.
6. **Lindesmith LC, Debbink K, Swanstrom J, Vinje J, Costantini V, Baric RS, Donaldson EF.** 2012. Monoclonal antibody-based antigenic mapping of norovirus GII.4-2002. J Virol **86:**873–883. http://dx.doi.org/10.1128/JVI.06200-11.
7. **Lindesmith LC, Donaldson EF, Lobue AD, Cannon JL, Zheng DP, Vinje J, Baric RS.** 2008. Mechanisms of GII.4 norovirus persistence in human populations. PLoS Med **5:**e31. http://dx.doi.org/10.1371/journal.pmed.0050031.
8. **Jones MK, Watanabe M, Zhu S, Graves CL, Keyes LR, Grau KR, Gonzalez-Hernandez MB, Iovine NM, Wobus CE, Vinje J, Tibbetts SA, Wallet SM, Karst SM.** 2014. Enteric bacteria promote human and mouse

norovirus infection of B cells. Science **346:**755–759. http://dx.doi.org/10.1126/science.1257147.
9. **Prasad BV, Hardy ME, Dokland T, Bella J, Rossmann MG, Estes MK.** 1999. X-ray crystallographic structure of the Norwalk virus capsid. Science **286:**287–290. http://dx.doi.org/10.1126/science.286.5438.287.
10. **Katpally U, Voss NR, Cavazza T, Taube S, Rubin JR, Young VL, Stuckey J, Ward VK, Virgin HW, Wobus CE, Smith TJ.** 2010. High-resolution cryo-electron microscopy structures of murine norovirus 1 and rabbit hemorrhagic disease virus reveal marked flexibility in the receptor binding domains. J Virol **84:**5836–5841. http://dx.doi.org/10.1128/JVI.00314-10.
11. **Hansman GS, Taylor DW, McLellan JS, Smith TJ, Georgiev I, Tame JR, Park SY, Yamazaki M, Gondaira F, Miki M, Katayama K, Murata K, Kwong PD.** 2012. Structural basis for broad detection of genogroup II noroviruses by a monoclonal antibody that binds to a site occluded in the viral particle. J Virol **86:**3635–3646. http://dx.doi.org/10.1128/JVI.06868-11.
12. **Smith TJ.** 2011. Structural studies on antibody recognition and neutralization of viruses. Curr Opin Virol **1:**150–156. http://dx.doi.org/10.1016/j.coviro.2011.05.020.
13. **Parker TD, Kitamoto N, Tanaka T, Hutson AM, Estes MK.** 2005. Identification of genogroup I and genogroup II broadly reactive epitopes on the norovirus capsid. J Virol **79:**7402–7409. http://dx.doi.org/10.1128/JVI.79.12.7402-7409.2005.
14. **Shiota T, Okame M, Takanashi S, Khamrin P, Takagi M, Satou K, Masuoka Y, Yagyu F, Shimizu Y, Kohno H, Mizuguchi M, Okitsu S, Ushijima H.** 2007. Characterization of a broadly reactive monoclonal antibody against norovirus genogroups I and II: recognition of a novel conformational epitope. J Virol **81:**12298–12306. http://dx.doi.org/10.1128/JVI.00891-07.
15. **Hansman GS, Doan LT, Kguyen TA, Okitsu S, Katayama K, Ogawa S, Natori K, Takeda N, Kato Y, Nishio O, Noda M, Ushijima H.** 2004. Detection of norovirus and sapovirus infection among children with gastroenteritis in Ho Chi Minh City, Vietnam. Arch Virol **149:**1673–1688. http://dx.doi.org/10.1007/s00705-004-0345-4.
16. **Koho T, Huhti L, Blazevic V, Nurminen K, Butcher SJ, Laurinmäki P, Kalkkinen N, Rönnholm G, Vesikari T, Hytönen VP, Kulomaa MS.** 2012. Production and characterization of virus-like particles and the P domain protein of GII.4 norovirus. J Virol Methods **179:**1–7. http://dx.doi.org/10.1016/j.jviromet.2011.05.009.
17. **Hansman GS, Biertumpfel C, Georgiev I, McLellan JS, Chen L, Zhou T, Katayama K, Kwong PD.** 2011. Crystal structures of GII.10 and GII.12 norovirus protruding domains in complex with histo-blood group antigens reveal details for a potential site of vulnerability. J Virol **85:**6687–6701. http://dx.doi.org/10.1128/JVI.00246-11.
18. **Hansman GS, Guntapong R, Pongsuwanna Y, Natori K, Katayama K, Takeda N.** 2006. Development of an antigen ELISA to detect sapovirus in clinical stool specimens. Arch Virol **151:**551–561. http://dx.doi.org/10.1007/s00705-005-0630-x.
19. **Hansman GS, Katayama K, Maneekarn N, Peerakome S, Khamrin P, Tonusin S, Okitsu S, Nishio O, Takeda N, Ushijima H.** 2004. Genetic diversity of norovirus and sapovirus in hospitalized infants with sporadic cases of acute gastroenteritis in Chiang Mai, Thailand. J Clin Microbiol **42:**1305–1307. http://dx.doi.org/10.1128/JCM.42.3.1305-1307.2004.
20. **Bull RA, Tu ET, McIver CJ, Rawlinson WD, White PA.** 2006. Emergence of a new norovirus genotype II.4 variant associated with global outbreaks of gastroenteritis. J Clin Microbiol **44:**327–333. http://dx.doi.org/10.1128/JCM.44.2.327-333.2006.
21. **Kabsch W.** 1993. Automatic processing of rotation diffraction data from crystals of initially unknown symmetry and cell constants. J Appl Crystallogr **26:**795–800. http://dx.doi.org/10.1107/S0021889893005588.
22. **McCoy AJ, Grosse-Kunstleve RW, Adams PD, Winn MD, Storoni LC, Read RJ.** 2007. Phaser crystallographic software. J Appl Crystallogr **40:**658–674. http://dx.doi.org/10.1107/S0021889807021206.
23. **Emsley P, Lohkamp B, Scott WG, Cowtan K.** 2010. Features and development of Coot. Acta Crystallogr D Biol Crystallogr **66:**486–501. http://dx.doi.org/10.1107/S0907444910007493.
24. **Adams PD, Afonine PV, Bunkóczi G, Chen VB, Davis IW, Echols N, Headd JJ, Hung L-W, Kapral GJ, Grosse-Kunstleve RW, McCoy AJ, Moriarty NW, Oeffner R, Read RJ, Richardson DC, Richardson JS, Terwilliger TC, Zwart PH.** 2010. PHENIX: a comprehensive Python-based system for macromolecular structure solution. Acta Crystallogr D Biol Crystallogr **66:**213–221. http://dx.doi.org/10.1107/S0907444909052925.
25. **Morris AL, MacArthur MW, Hutchinson EG, Thornton JM.** 1992. Stereochemical quality of protein structure coordinates. Proteins **12:**345–364. http://dx.doi.org/10.1002/prot.340120407.
26. **Chen VB, Arendall WB, III, Headd JJ, Keedy DA, Immormino RM, Kapral GJ, Murray LW, Richardson JS, Richardson DC.** 2010. MolProbity: all-atom structure validation for macromolecular crystallography. Acta Crystallogr D Biol Crystallogr **66:**12–21. http://dx.doi.org/10.1107/S0907444909042073.
27. **Krissinel E, Henrick K.** 2007. Inference of macromolecular assemblies from crystalline state. J Mol Biol **372:**774–797. http://dx.doi.org/10.1016/j.jmb.2007.05.022.
28. **Spinelli S, Frenken L, Bourgeois D, de Ron L, Bos W, Verrips T, Anguille C, Cambillau C, Tegonil M.** 1996. The crystal structure of a llama heavy chain variable domain. Nat Struct Biol **3:**752–757. http://dx.doi.org/10.1038/nsb0996-752.
29. **Desmyter A, Transue TR, Ghahroudi MA, Thi MH, Poortmans F, Hamers R, Muyldermans S, Wyns L.** 1996. Crystal structure of a camel single-domain VH antibody fragment in complex with lysozyme. Nat Struct Biol **3:**803–811. http://dx.doi.org/10.1038/nsb0996-803.
30. **Helma J, Schmidthals K, Lux V, Nuške S, Scholz AM, Kraüsslich HG, Rothbauer U, Leonhardt H.** 2012. Direct and dynamic detection of HIV-1 in living cells. PLoS One **7:**e50026. http://dx.doi.org/10.1371/journal.pone.0050026.
31. **De Meyer T, Muyldermans S, Depicker A.** 2014. Nanobody-based products as research and diagnostic tools. Trends Biotechnol **32:**263–270. http://dx.doi.org/10.1016/j.tibtech.2014.03.001.
32. **Goldman ER, Anderson GP, Liu JL, Delehanty JB, Sherwood LJ, Osborn LE, Cummins LB, Hayhurst A.** 2006. Facile generation of heat-stable antiviral and antitoxin single domain antibodies from a semisynthetic llama library. Anal Chem **78:**8245–8255. http://dx.doi.org/10.1021/ac0610053.
33. **Sherwood LJ, Osborn LE, Carrion R, Jr, Patterson JL, Hayhurst A.** 2007. Rapid assembly of sensitive antigen-capture assays for Marburg virus, using in vitro selection of llama single-domain antibodies, at biosafety level 4. J Infect Dis **196**(Suppl 2)**:**S213–S219. http://dx.doi.org/10.1086/520586.
34. **Fatima A, Wang H, Kang K, Xia L, Wang Y, Ye W, Wang J, Wang X.** 2014. Development of VHH antibodies against dengue virus type 2 NS1 and comparison with monoclonal antibodies for use in immunological diagnosis. PLoS One **9:**e95263. http://dx.doi.org/10.1371/journal.pone.0095263.
35. **Ibanez LI, De Filette M, Hultberg A, Verrips T, Temperton N, Weiss RA, Vandevelde W, Schepens B, Vanlandschoot P, Saelens X.** 2011. Nanobodies with in vitro neutralizing activity protect mice against H5N1 influenza virus infection. J Infect Dis **203:**1063–1072. http://dx.doi.org/10.1093/infdis/jiq168.
36. **Wei G, Meng W, Guo H, Pan W, Liu J, Peng T, Chen L, Chen CY.** 2011. Potent neutralization of influenza A virus by a single-domain antibody blocking M2 ion channel protein. PLoS One **6:**e28309. http://dx.doi.org/10.1371/journal.pone.0028309.
37. **Hinz A, Lutje Hulsik D, Forsman A, Koh WW, Belrhali H, Gorlani A, de Haard H, Weiss RA, Verrips T, Weissenhorn W.** 2010. Crystal structure of the neutralizing llama VHH D7 and its mode of HIV-1 gp120 interaction. PLoS One **5:**e10482. http://dx.doi.org/10.1371/journal.pone.0010482.
38. **De Meyer T, Muyldermans S, Depicker A.** 2014. Nanobody-based products as research and diagnostic tools. Trends Biotechnol **32:**263–270. http://dx.doi.org/10.1016/j.tibtech.2014.03.001.
39. **de Bruin E, Duizer E, Vennema H, Koopmans MP.** 2006. Diagnosis of norovirus outbreaks by commercial ELISA or RT-PCR. J Virol Methods **137:**259–264. http://dx.doi.org/10.1016/j.jviromet.2006.06.024.
40. **Burton-MacLeod JA, Kane EM, Beard RS, Hadley LA, Glass RI, Ando T.** 2004. Evaluation and comparison of two commercial enzyme-linked immunosorbent assay kits for detection of antigenically diverse human noroviruses in stool samples. J Clin Microbiol **42:**2587–2595. http://dx.doi.org/10.1128/JCM.42.6.2587-2595.2004.
41. **Kele B, Lengyel G, Deak J.** 2011. Comparison of an ELISA and two reverse transcription polymerase chain reaction methods for norovirus detection. Diagn Microbiol Infect Dis **70:**475–478. http://dx.doi.org/10.1016/j.diagmicrobio.2011.04.002.
42. **Singh BK, Leuthold MM, Hansman GS.** 2015. Human noroviruses' fondness for histo-blood group antigens. J Virol **89:**2024–2040. http://dx.doi.org/10.1128/JVI.02968-14.